Enhancements of Himalayan and Tibetan Erosion and the Produced Organic Carbon Burial in Distal Tropical Marginal Seas During the Quaternary Glacial Periods: An Integration of Sedimentary Records

Zhaokai Xu, Shiming Wan, Christophe Colin, Peter D. Clift, Fengming Chang, Tiegang Li, Hongjin Chen, Mingjiang Cai, Zhaojie Yu, Dhongil Lim

▶ **To cite this version:**

Zhaokai Xu, Shiming Wan, Christophe Colin, Peter D. Clift, Fengming Chang, et al.. Enhancements of Himalayan and Tibetan Erosion and the Produced Organic Carbon Burial in Distal Tropical Marginal Seas During the Quaternary Glacial Periods: An Integration of Sedimentary Records. Journal of Geophysical Research: Earth Surface, 2021, 126, 10.1029/2020JF005828 . insu-03745272

HAL Id: insu-03745272
https://insu.hal.science/insu-03745272

Submitted on 4 Aug 2022

HAL is a multi-disciplinary open access archive for the deposit and dissemination of scientific research documents, whether they are published or not. The documents may come from teaching and research institutions in France or abroad, or from public or private research centers.

L'archive ouverte pluridisciplinaire **HAL**, est destinée au dépôt et à la diffusion de documents scientifiques de niveau recherche, publiés ou non, émanant des établissements d'enseignement et de recherche français ou étrangers, des laboratoires publics ou privés.

Copyright

Correspondence to:
Z. Xu, T. Li, and D. Lim,
zhaokaixu@qdio.ac.cn;
tgli@fio.org.cn;
oceanlim@kiost.ac.kr

Enhancements of Himalayan and Tibetan Erosion and the Produced Organic Carbon Burial in Distal Tropical Marginal Seas During the Quaternary Glacial Periods: An Integration of Sedimentary Records

Zhaokai Xu[1,2,3,4] , Shiming Wan[1,2,4], Christophe Colin[5] , Peter D. Clift[6] , Fengming Chang[1,2,3] , Tiegang Li[2,7], Hongjin Chen[1,8], Mingjiang Cai[1,8], Zhaojie Yu[1,2,3] , and Dhongil Lim[9]

[1]CAS Key Laboratory of Marine Geology and Environment, Institute of Oceanology, Chinese Academy of Sciences, Qingdao, China, [2]Laboratory for Marine Geology, Pilot National Laboratory for Marine Science and Technology, Qingdao, China, [3]Center for Ocean Mega-Science, Chinese Academy of Sciences, Qingdao, China, [4]CAS Center for Excellence in Quaternary Science and Global Change, Xi'an, China, [5]Laboratoire Geosciences Paris-Sud (GEOPS), CNRS-Université de Paris-Sud, Université Paris-Saclay, Orsay Cedex, France, [6]Department of Geology and Geophysics, Louisiana State University, Baton Rouge, LA, USA, [7]Key Laboratory of Marine Sedimentology and Environmental Geology, First Institute of Oceanography, Ministry of Natural Resources, Qingdao, China, [8]University of Chinese Academy of Sciences, Beijing, China, [9]South Sea Research Institute, Korea Institute of Ocean Science & Technology, Geoje, Republic of Korea

Abstract The Himalayan and Tibetan highlands (mountains), with high rates of physical erosion, are extreme settings for earth surface processes, generating one of the largest recent terrigenous detritus and organic carbon discharges to the ocean. However, their significance with respect to the global carbon and climate cycles during the Quaternary is still unclear, especially in quantitative terms. Here, we present comprehensive records of continental erosion and weathering, terrestrial supply, marine productivity, and organic carbon burial in the distal Arabian Sea, Bay of Bengal, and southern South China Sea since ~700 ka over orbital timescales. These records exhibit periodicities corresponding to sea level and Indian summer monsoon intensity changes. During glacial periods, the enhanced highland surface erosion and activation of deep-sea channels significantly increased inputs of terrigenous detritus, nutrients, and organic carbon into the Arabian Sea and Bay of Bengal, whereas strengthened continental shelf surface weathering and organic matter preservation occurred in the South China Sea. Conclusively, our integrative proxies in the study area demonstrate, for the first time, pronounced glacial burial pulses of organic carbon ($\sim 1.12 \times 10^{12}$ mol/yr), dominantly originating from the highland surface erosion and marine productivity. Together with the increased silicate weathering on the exposed tropical continental shelves and in the tropical volcanic arcs, the enhanced burial flux of organic carbon in the tropical marginal seas, therefore, highlights the large contributions that tropical regions can make within the glacial-interglacial carbon inventory of the ocean and atmosphere and thus cause significant negative feedback on the global climate.

Plain Language Summary Anthropogenic emissions of the greenhouse gas CO_2 are significantly changing the global climate and environment, resulting in a warmer state for which there is no historical analog. Marine records hold valuable lessons for the future of our warming world, as marine sediments are an important reservoir of the global organic carbon and then modulate release of CO_2 into the atmosphere. Currently, the major river systems originating from the Himalaya and Tibetan Plateau discharge ~25% of the global fluvial sediment flux to the ocean, acting as an important source of continental organic carbon at tectonic and current timescales. Our integrative mineralogical-geochemical study demonstrates the enhanced highland (mountain) erosion and activation of deep-sea channels, increased supplies of the produced materials, strengthened marine productivity, and effective preservation of organic carbon in the deep Arabian Sea and Bay of Bengal during cold periods. In contrast, strengthened chemical decomposition of silicates on the exposed continental shelf was coeval with increased organic carbon storage in the deep South China Sea. The study area contributed ~1/4 of the current global marine burial flux of organic carbon during sea-level lowstands and thus represents a key precedent for understanding increasingly severe global warming.

1. Introduction

Globally, approximately 20–45% of terrestrial organic carbon delivered to the ocean by rivers is estimated to be buried in marine sediments, especially in continental margins (Bianchi & Allison, 2009; Blair & Aller, 2012; Burdige, 2005; Walsh, 1991; Zhao et al., 2020). The mountain range of Himalaya and Tibetan Plateau, with high rates of physical erosion generally associated with rock uplift and Indian winter monsoon climate variations, were extreme settings for earth surface processes during the Quaternary sea-level lowstands with respect to the eccentricity (100 kyr) periodicity (Chen et al., 2019a, 2020; Weber et al., 2018; Yu et al., 2019). In addition, the Indian summer monsoon climate, which is characterized by the strong precession (22 kyr) periodicity, significantly influences chemical weathering and organic carbon destabilization in the Himalayan and Tibetan lowlands during the Quaternary interglacial periods (Chen, Xu et al., 2019, 2020; Hein et al., 2020). These processes generate the largest sediment discharge to the ocean, ~25% of the global fluvial sediment flux, through several major river systems, including the Yellow and Yangtze Rivers in the east, the Indus River in the west, and the Ganges, Brahmaputra, Irrawaddy, Salween, and Mekong Rivers in the south (Figure 1; Liu et al., 2020; Milliman & Farnsworth, 2011). Among them, the Irrawaddy and Salween Rivers annually transport 1.9 Mt organic carbon to the sea, suggesting that these rivers may currently be one of the largest riverine sources of organic carbon (Baronas et al., 2020). High sedimentation rates and reduced oxygen exposure of terrigenous matter, as well as a persistent oxygen minimum zone on the continental margins adjacent to these major rivers, sustain the high burial efficiency of terrestrial organic matter both currently (70–85%; Galy et al., 2007) and during the Last Glacial Maximum and late marine isotope stage 6 (Cartapanis et al., 2016; D′Asaro et al., 2020; Kim et al., 2018). Quantitatively, the Bengal Fan currently accounts for ~10–20% of the total terrigenous organic carbon buried in marine sediments
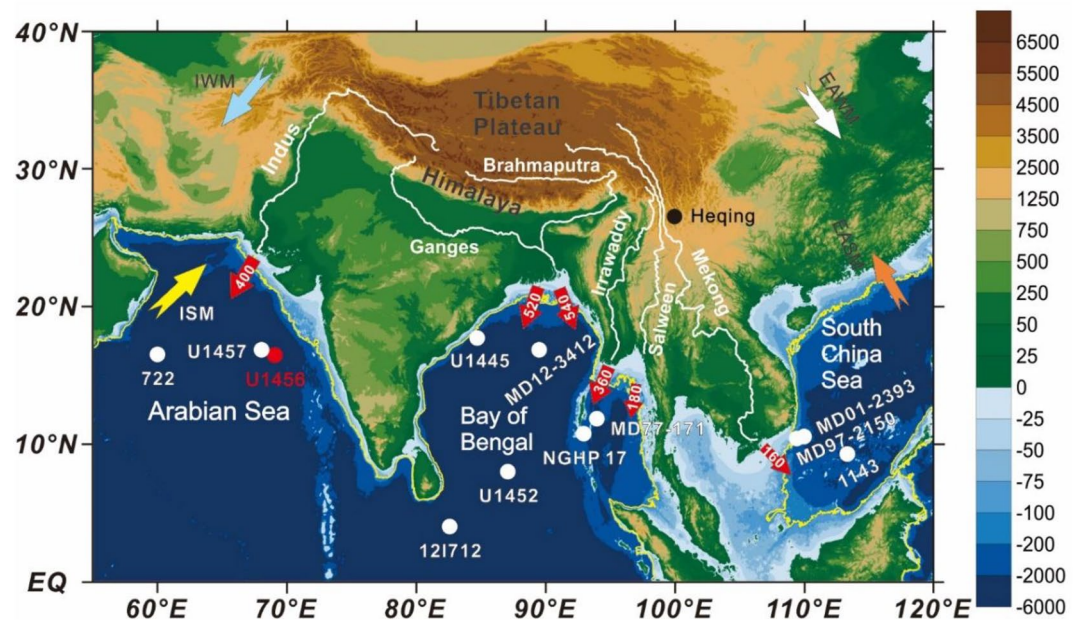

Figure 1. Bathymetric map showing the locations of IODP Site U1456 (Pandey et al., 2016) and representative reference sediment cores (Ocean Drilling Program, ODP, Site 722 from Clemens et al., 1996; IODP Site U1457 from Yu et al., 2019, Heqing Basin from An et al., 2011; IODP Site U1445 from Lee et al., 2020; MD12-3412 from Joussain et al., 2016 and Fauquembergue et al., 2019; MD77-171 from Yu et al., 2020; NGHP 17 from Gebregiorgis et al., 2018; IODP Site U1452 from Weber et al., 2018; 12I712 from Liu et al., 2019; MD97-2150 and MD01-2393 from Liu et al., 2004; and ODP Site 1143 from Wang et al., 2005 and Wan et al., 2017; dots) in the distal tropical Arabian Sea, Bay of Bengal, and southern South China Sea, as well as surrounding landmasses. The modern monsoon directions (arrows), major rivers (white lines), and annual fluvial sediment discharges (Mt/yr) of these rivers (Liu et al., 2020; Milliman & Farnsworth, 2011; arrows with numbers) in the study area are also shown. Note the potential seaward progradation of the paleocoastline to near the −100-m isobath (yellow lines) during the Quaternary glacial periods (Bintanja et al., 2005), leading to greater exposure of the continental shelf in the southern South China Sea than in other areas. EQ = equator, ISM = Indian summer monsoon, IWM = Indian winter monsoon, EASM = East Asian summer monsoon, EAWM = East Asian winter monsoon.

(Galy et al., 2007), which may be more important as a mechanism for buffering the atmospheric CO_2 level than chemical weathering of Himalayan and Tibetan silicates during the Neogene over tectonic timescales (France-Lanord & Derry, 1997). The recent research of Hilton (2017) and Hilton and West (2020), derived from geologic settings different from that of the current study (e.g., Taiwan and Guadeloupe), further emphasizes the potentially close but complex associations among mountain building, silicate erosion and weathering, the carbon cycle, and Earth's long-term climate.

Unfortunately, the significance of highland erosion for explaining the very large terrigenous organic carbon deposition in the eastern Arabian Sea and Bay of Bengal, together with the potential contributions to global change, during the Quaternary over orbital timescales has not been quantitatively evaluated (Cartapanis et al., 2016; Weber et al., 2018). In addition, a recent study in the South China Sea emphasizes the significance of glacial weathering of silicates on the exposed tropical continental shelves, partly originating from the Himalaya and Tibetan Plateau, for the sequestration of atmospheric CO_2 during the Quaternary (Wan et al., 2017). Furthermore, the more recent research in the western Philippine Sea indicates the important role of silicate weathering in the tropical volcanic arcs in the global climate change due to atmospheric CO_2 consumption during the Quaternary sea-level lowstands (Xu et al., 2018, 2020). Therefore, little is known regarding the exact relationship between physical erosion and chemical weathering of silicates originating from the Himalaya and Tibetan Plateau and the inputs and burial of the produced detritus and organic carbon in different tropical marginal seas surrounding these highlands (mountains) during the Quaternary over orbital timescales (Hein et al., 2020). Their potential significance for the global carbon cycle is also unknown due to a lack of comprehensive and quantitative sedimentary records in the sea, especially in the eastern Arabian Sea and Bay of Bengal. The contributions of tropical regions to the global climate variability through atmospheric CO_2 consumption and terrestrial organic carbon burial in marine sediments may be underestimated.

Many studies have revealed that illite and chlorite transported by the Indus, Ganges, and Brahmaputra Rivers to the eastern Arabian Sea, Bay of Bengal, and southern South China Sea during the Quaternary are representative products of physical erosion in the Himalayan and Tibetan highlands, whereas smectite is dominantly derived from chemical weathering in the surrounding floodplains or volcanic rock regions and is then transported to the seas by rivers in India and the Philippines (Chen, Xu, et al., 2019; Colin et al, 1999, 2010; Joussain et al., 2016; Liu et al., 2004, 2019; Wan et al., 2012). These clay minerals effectively help transport and bury terrigenous organic carbon in the marine realm (Blattmann et al., 2019; France-Lanord & Derry, 1997). The (illite + chlorite)/smectite ratio and $(Al/K)_{sample}/(Al/K)_{upper\ continental\ crust}$ ratio can be used to decode highland erosion relative to lowland weathering (Chen et al., 2020; Colin et al., 2006; Yu et al., 2020), and Sr-Nd isotope compositions are suitable proxies to trace terrestrial sediment provenance (Khim et al., 2018; Yu et al., 2019). In addition, contents, ratios, and fluxes of geochemical compositions, such as biogenic silica, total organic carbon, and molar ratio of total organic carbon to total nitrogen, have been conventionally applied to constrain the sea surface productivity level and the origin of organic matter in marine sediments (Lee et al., 2020; Lim et al., 2011; Ramaswamy et al., 2008; Rixen et al., 2019; Xu et al., 2020). In particular, the high correlation coefficient value between the ratio of total organic carbon to total nitrogen and $\delta^{13}C$ value of organic matter (correlation coefficient of 0.93, $p < 0.05$) for the upper continuous and homogeneous sediments at International Ocean Discovery Program (IODP) Site U1452 in the Bay of Bengal clearly demonstrates that higher ratios of total organic carbon to total nitrogen indicate increased inputs of terrigenous organic carbon during glacial periods (Weber et al., 2018). This deduction is supported by the generally positive correlation (correlation coefficient of 0.50, $p < 0.05$) between these two proxies at IODP Site U1445 in the Bay of Bengal since ~700 ka (Lee et al., 2020). In general, typical terrestrial and marine organic matter have ratios of total organic carbon to total nitrogen >10 and ~6, respectively (Lim et al., 2011 and references therein).

In this study, we conducted the first comprehensive investigation of various proxy records for physical erosion and chemical weathering associated with the Himalaya and Tibetan Plateau using the terrestrial detritus and organic matter compositions in the distal tropical Arabian Sea, Bay of Bengal, and southern South China Sea (Figure 1). New data (Table 1) and previously published sedimentary and geochemical indicators (Tables 1–3) from 13 sediment cores in these seas (An et al., 2011; Cai et al, 2018, 2019; Chen, Xu et al, 2019, 2020; Clemens et al., 1996; Fauquembergue et al., 2019; Gebregiorgis et al., 2018; Joussain et al., 2016; Khim

Table 1
Average Values of Some Typical Proxies at IODP Site U1456 (Cai et al., 2018, 2019; Chen, Xu et al., 2019, 2020; Khim et al., 2018)

Period	Age (ka)	(Illite + chlorite)/ smectite	$(Al/K)_{sample}$/(Al/K) upper continental crust	MAR_{Indus} (g/ cm^2/kyr)	ε_{Nd}	MAR_{BSi} (g/ cm^2/kyr)	MAR_{TOC} (g/ cm^2/kyr)	TOC/TN
MIS 1	0–14	1.2 (0.6)	1.38 (0.16)	0.9 (0.4)	−10.0 (2.5)	0.07 (0.03)	0.05 (0.03)	8.3 (2.0)
MIS 2–4	14–71	0.8 (0.3)	1.23 (0.03)	1.0 (0.3)	−10.3 (0.7)	0.06 (0.02)	0.05 (0.02)	9.5 (1.2)
MIS 5	71–130	0.6 (0.3)	1.33 (0.09)	1.5 (0.9)	−10.9 (1.5)	0.06 (0.05)	0.03 (0.02)	7.6 (2.1)
MIS 6	130–191	0.6 (0.5)	1.36 (0.09)	4.6 (2.5)	−10.9 (1.5)	0.25 (0.16)	0.09 (0.05)	8.5 (2.8)
MIS 7	191–243	0.6 (0.3)	1.25 (0.11)	2.1 (0.8)	−10.7 (0.8)	0.12 (0.04)	0.05 (0.05)	7.1 (2.9)
MIS 8	243–300	0.5 (0.3)	1.27 (0.13)	1.4 (0.4)	−10.1 (2.2)	0.12 (0.03)	0.07 (0.02)	7.9 (1.9)
MIS 9	300–337	0.3 (0.1)	1.39 (0.17)	0.7 (0.3)	−8.9 (1.0)	0.12 (0.07)	0.05 (0.03)	8.6 (1.3)
MIS 10	337–374	1.0 (0.6)	1.23 (0.12)	3.4 (1.1)	−11.5 (0.4)	0.20 (0.10)	0.15 (0.11)	9.0 (3.6)
MIS 11	374–424	0.7 (0.4)	1.38 (0.11)	1.4 (0.5)	−10.4 (0.9)	0.07 (0.01)	0.06 (0.03)	9.0 (1.2)
MIS 12	424–478	1.8 (0.9)	1.17 (0.10)	6.7 (4.4)	−10.9 (0.3)	0.08 (0.02)	0.07 (0.03)	8.5 (1.0)
MIS 13	478–533	0.4 (0.2)	1.31 (0.15)	5.7 (3.4)	−12.0 (2.2)	0.25 (0.12)	0.15 (0.08)	8.8 (1.7)
MIS 14	533–563	0.4 (0.1)	1.46 (0.15)	2.1 (0.4)	−10.2 (0.4)	0.20 (0.15)	0.07 (0.02)	10.0 (1.7)
MIS 15	563–621	0.6 (0.3)	1.31 (0.09)	1.3 (0.7)	−8.6 (0.04)	0.22 (0.11)	0.09 (0.05)	9.3 (1.3)
MIS 16	621–676	0.8 (0.5)	1.30 (0.09)	1.2 (0.5)	−9.4 (0.4)	0.12 (0.05)	0.11 (0.03)	10.9 (2.1)
MIS 17	676–698	0.3 (0.1)	1.41 (0.08)	1.4 (0.7)	−9.8	0.11 (0.07)	0.07 (0.01)	10.0 (4.1)
Interglacial	-	0.7 (0.4)	1.33 (0.13)	1.4 (0.8)	−10.2 (1.3)	0.10 (0.07)	0.05 (0.04)	8.2 (2.3)
Glacial	-	0.8 (0.6)	1.29 (0.13)	3.1 (2.9)	−10.5 (1.2)	0.14 (0.12)	0.08 (0.05)	9.1 (2.2)
Glacial/interglacial	-	1.3	1.0	2.2	1.0	1.4	1.5	1.1
Glacial/current (core top)	-	1.3	0.8	3.1	0.8	1.1	2.1	1.4

Notes. The number in parentheses is the standard deviation. Marine isotope stage (MIS) 13 is excluded from the interglacial calculation. MAR_{Indus} = mass accumulation rate of the Indus River detritus. MAR_{BSi} = mass accumulation rate of biogenic silica. MAR_{TOC} = mass accumulation rate of total organic carbon. TOC/TN = ratio of total organic carbon to total nitrogen.

et al., 2018; Kim et al., 2018; Lee et al., 2020; Liu et al., 2004, 2019; Tripathi et al., 2017; Wan et al., 2017; Wang et al., 2005; Weber et al., 2018; Yu et al, 2019, 2020) were integrated to establish temporal and spatial variations in the abovementioned processes, together with the associations among them. We also provide new insights into the quantitative significance of organic carbon burial in the study area for the global carbon and climate cycles during the Quaternary over orbital timescales. Hence, the total quantitative contributions of tropical regions to the global climate change due to atmospheric CO_2 consumption associated with continental silicate weathering (Wan et al., 2017; Xu et al., 2018, 2020) and terrestrial organic carbon burial in marine sediments dominantly derived from silicate erosion in the Himalayan and Tibetan highlands (France-Lanord & Derry, 1997; Galy et al., 2007; Lee et al., 2020; Weber et al., 2018) can be better constrained, especially during the Quaternary glacial periods (Cartapanis et al., 2016).

2. Materials and Methods

IODP Site U1456 is located in the Laxmi Basin in the eastern Arabian Sea (16°37.28′N, 68°50.33′E) at a water depth of 3,640 m (Figure 1). Here, we focus on the upper 82.02 m of core (composite depth below the seafloor) at IODP Site U1456 with an average linear sedimentation rate of ~11.8 cm/kyr, which is characterized by strong eccentricity (100 kyr) and precession (22 kyr) periodicities in continental erosion and weathering proxies beginning at ~700 ka (Cai et al., 2018, 2019; Chen, Xu et al., 2019, 2020). Sr-Nd isotope compositions of the clay-sized (<2 µm) detrital sediment fractions for 12 new samples, together with concentrations of total organic carbon, total nitrogen, and biogenic silica for 101 new samples, were measured using the same analytical methods and accuracy reported by Chen et al. (2020) and Xu et al. (2020), to better constrain sediment provenance and marine productivity, as well as the origin and burial of organic carbon.

Table 2
Dominant Proxies, Cited in This Study, for the Representative Reference Sediment Cores Collected From the Distal Tropical Arabian Sea, Bay of Bengal, and Southern South China Sea, as Well as Surrounding Landmasses (Figure 1)

Region	Site	Proxies	References
Western Arabian Sea	ODP Site 722	Mass accumulation rates of eolian dust and total organic carbon	Clemens et al. (1996)
Eastern Arabian Sea	IODP Site U1457	(Illite + chlorite)/smectite ratio, ε_{Nd}, and turbidite frequency	Yu et al. (2019)
Heqing Basin	Heqing	Indian summer monsoon index	An et al. (2011)
Bay of Bengal	IODP Site U1445	$\delta^{13}C$ value of organic matter, as well as contents and mass accumulation rates of total organic carbon, total nitrogen, and biogenic silica	Lee et al. (2020)
	MD12-3412	(Illite + chlorite)/smectite ratio, ε_{Nd}, and turbidite frequency	Joussain et al. (2016); Fauquembergue et al. (2019)
	MD77-171	(Illite + chlorite)/smectite ratio	Yu et al. (2020)
	NGHP 17	$\delta^{18}O$ value of sea water	Gebregiorgis et al. (2018)
	IODP Site U1452	Linear sedimentation rate, $\delta^{13}C$ value of organic matter, and contents of total organic carbon, total nitrogen, Ti, and biologic Ca	Weber et al. (2018)
	12I712	ε_{Nd}	Liu et al. (2019)
Southern South China Sea (slope)	MD97-2150 and MD01-2393	Linear sedimentation rate and (illite + chlorite)/smectite ratio	Liu et al. (2004)
Southern South China Sea (deep sea)	ODP Site 1143	(Illite + chlorite)/smectite ratio, $(Al/K)_{sample}/(Al/K)_{upper\ continental\ crust}$ ratio, ε_{Nd}, contents of total organic carbon and total nitrogen, and mass accumulation rates of terrigenous detritus and total organic carbon	Wang et al. (2005); Wan et al. (2017)

Sr-Nd isotope analysis samples were chosen from the key gap layers existing at IODP Site U1456 in previous studies (Cai et al., 2019; Chen et al., 2020; Khim et al., 2018). The bulk sediment was treated with deionized water, 10% acetic acid, a mixture of 1 mol/L hydroxylamine hydrochloride and 25% acetic acid, 5% hydrogen peroxide, and 2 mol/L sodium carbonate to extract the detrital sediment fraction. Subsequently, the clay-sized detrital particles were isolated by centrifugation following Stokes' settling principle. Approximately 0.1 g of detritus produced from each sample was powdered, completely digested in a mixed solution of nitric acid, hydrofluoric acid, and perchloric acid on a hot plate, concentrated, and measured using a thermal ionization mass spectrometer (Phoenix) in the Analytical Laboratory, Beijing Research Institute of Uranium Geology. Analyses of the Sr standard NBS SRM987 and the Nd standard Shin Etsu JNdi-1 yielded an $^{87}Sr/^{86}Sr$ ratio of 0.710250 ± 0.000007 (recommended value: 0.710250) and a $^{143}Nd/^{144}Nd$ ratio of 0.512118 ± 0.000003 (recommended value: 0.512115), respectively. For convenience, the $^{143}Nd/^{144}Nd$ ratio is expressed as $\varepsilon_{Nd} = [(^{143}Nd/^{144}Nd_{sample})/0.512638 - 1] \times 10^4$ (Chen et al., 2020, and references therein).

Concentrations of total organic carbon, total nitrogen, and biogenic silica were analyzed in the South Sea Research Institute, Korea Institute of Ocean Science and Technology. The total carbon and total nitrogen contents were measured using a Carlo Erba Elemental Analyzer 1108. The total inorganic carbon concentration was analyzed by a CO_2 Coulometer (CM5014). The analyses featured a 5% relative analytical error. The total organic carbon content was calculated as the difference between the total carbon and total inorganic carbon concentrations. The biogenic silica content was measured using a wet alkaline extraction method and an inductively coupled plasma optical emission spectrometer (IRIS Intrepid II XSP), with a relative analytical error of <10% (Xu et al., 2020, and references therein).

Spectral analysis was performed on some representative proxies from IODP Site U1456 (silicate erosion and weathering, flux of the Indus river detritus, and marine productivity) using the "PAST 3.0" software to examine the evolution of the dominant periodicity and thus the potential controlling mechanisms underlying variations in these indicators. The irregularly sampled time series were linearly interpolated to produce an

Table 3
Average Values of Some Typical Proxies in the Representative Reference Sediment Cores (Clemens et al., 1996; Fauquembergue et al., 2019; Joussain et al., 2016; Liu et al., 2004; Wan et al., 2017; Wang et al., 2005; Weber et al., 2018; Yu et al., 2019)

Region	Site	Proxies	Interglacial	Glacial	Glacial/ Interglacial	Glacial/ current (core top)
Western Arabian Sea	ODP Site 722	MAR_{eolian} (g/cm^2/kyr)	0.6 (0.3)	1.3 (0.7)	2.1	1.8
		MAR_{TOC} (g/cm^2/kyr)	0.2 (0.1)	0.4 (0.2)	1.8	0.8
Eastern Arabian Sea	IODP Site U1457	(Illite + chlorite)/smectite	0.6 (0.4)	1.4 (1.3)	2.4	2.7
		Turbidite frequency	25	53	2.1	/
Bay of Bengal	MD12-3412 and IODP Site U1452	(Illite + chlorite)/smectite	1.1 (0.5)	2.7 (1.1)	2.5	3.5
		Turbidite frequency	15	76	5.1	/
		LSR (cm/kyr)	2.1	2.5	1.2	1.3
		TOC (%)	0.7 (0.4)	1.3 (0.4)	2.0	2.8
Southern South China Sea (slope)	MD01-2393	(Illite + chlorite)/smectite	1.4 (0.3)	1.9 (0.3)	1.4	1.5
		LSR (cm/kyr)	19.5	24.2	1.2	0.7
Southern South China Sea (deep sea)	ODP Site 1143	(Illite + chlorite)/smectite	1.4 (0.4)	1.5 (0.4)	1.1	1.1
		$(Al/K)_{sample}/(Al/K)_{upper\ continental\ crust}$	1.30 (0.12)	1.33 (0.10)	1.0	0.8
		$MAR_{terrigenous}$ (g/cm^2/kyr)	4.0 (2.1)	3.4 (1.5)	0.8	/
		MAR_{TOC} (mg/cm^2/kyr)	15.1 (10.2)	19.6 (9.5)	1.3	1.6

Notes. The number in parentheses is the standard deviation. Marine isotope stage (MIS) 13 is excluded from the interglacial calculation. MAR_{eolian} = mass accumulation rate of eolian dust. MAR_{TOC} = mass accumulation rate of total organic carbon. LSR = linear sedimentation rate. TOC = total organic carbon. $MAR_{terrigenous}$ = mass accumulation rate of terrigenous detritus.

average sample spacing for the record. Confidence intervals of 90% and 80% were used when performing the spectral analysis (Chen et al., 2020, and references therein).

New data and published results for IODP Site U1456 with different time intervals of 2.9–9.2 kyr (Cai et al., 2018, 2019; Chen, Xu et al., 2019, 2020; Khim et al., 2018; Kim et al., 2018; Tripathi et al., 2017), together with those in 12 selected reference sediment cores with generally large fluvial discharges originating from the Himalaya and Tibetan Plateau or abundant eolian dust supplies from surrounding landmasses, continuous sedimentation, and high-resolution age model and sampling interval (An et al., 2011; Clemens et al., 1996; Fauquembergue et al., 2019; Gebregiorgis et al., 2018; Joussain et al., 2016; Lee et al., 2020; Liu et al., 2004, 2019; Wan et al., 2017; Wang et al., 2005; Weber et al., 2018; Yu et al, 2019, 2020), were synthesized for the following discussion. In particular, the detailed processes related to the Himalayan highland erosion and lowland weathering, as well as their potential significance for terrestrial organic carbon transfer, delivery, and deposition in the Bay of Bengal during the Neogene over tectonic timescales and since 18 ka over millennial timescales, have been well constrained by France-Lanord and Derry (1997), Galy et al. (2007), and Hein et al. (2020). Here, these theories and data are extrapolated to discuss variations in the abovementioned proxies, together with their controlling mechanisms and paleoenvironmental significance, since ~700 ka over orbital timescales. In particular, we dominantly focus on the simplified comparison between the average status of glacial and interglacial periods rather than complex variations within a specific glacial (or interglacial) stage.

3. Results

3.1. IODP Site U1456

IODP Site U1456 is characterized by orbital timescale changes in its clay mineralogy and geochemical compositions since ~700 ka (Figure 2; Table 1). In general, glacial sediments display higher average values of the (illite + chlorite)/smectite ratio, $^{87}Sr/^{86}Sr$ ratio, ratio of total organic carbon to total nitrogen, and mass
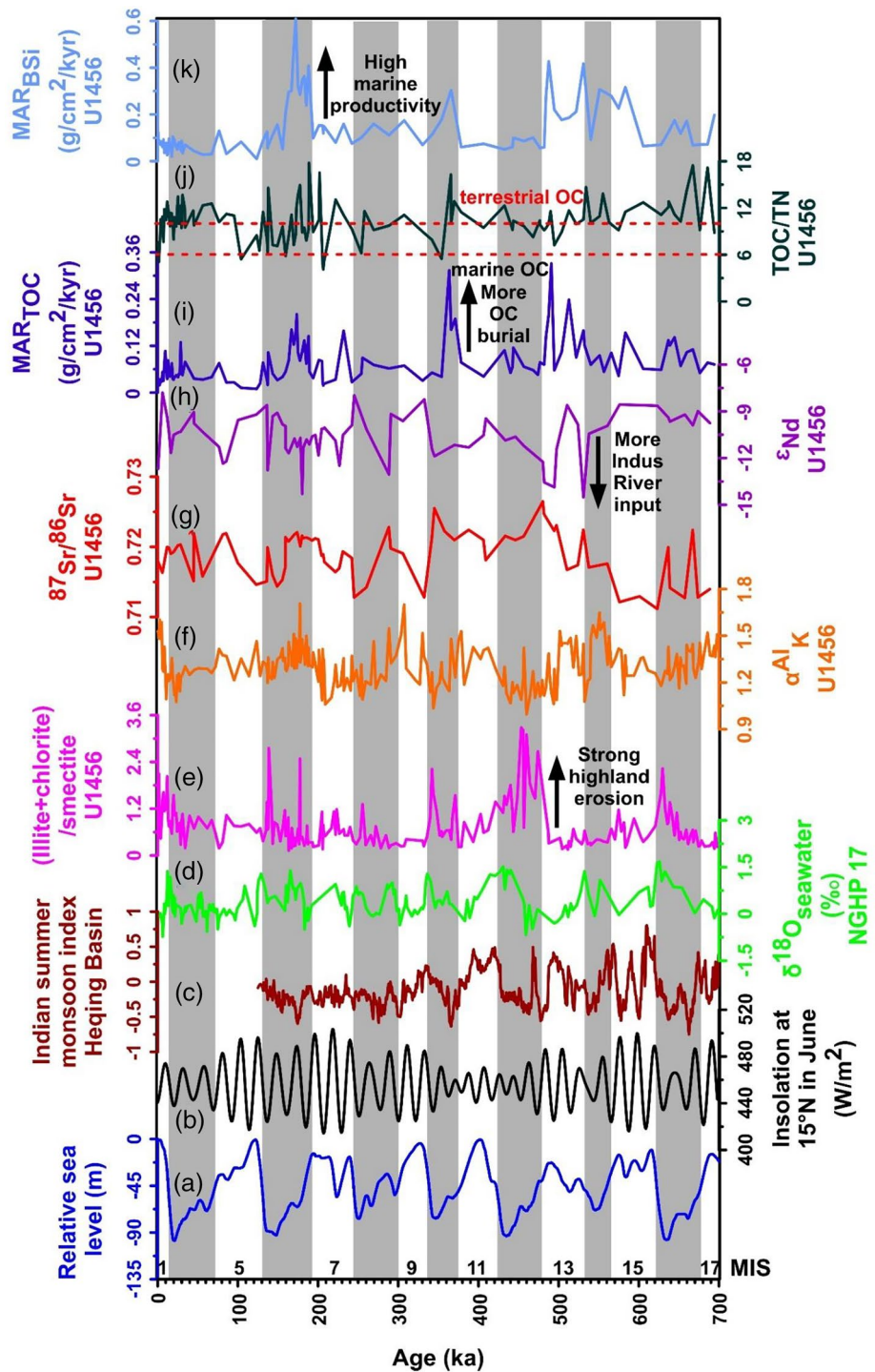
Figure 2. Comparison among (e) (illite + chlorite)/smectite ratio (Cai et al., 2018; Chen, Xu, et al., 2019), (f) $(Al/K)_{sample}/(Al/K)_{upper\ continental\ crust}$ ratio (α^{Al}_K; Cai et al., 2019; Chen et al., 2020), (g) $^{87}Sr/^{86}Sr$ ratio (Cai et al., 2019; Chen et al., 2020; Khim et al., 2018), (h) ε_{Nd} (Cai et al., 2019; Chen et al., 2020; Khim et al., 2018), (i) mass accumulation rate of total organic carbon (MAR_{TOC}), (j) ratio of total organic carbon to total nitrogen (TOC/TN), and (k) mass accumulation rate of biogenic silica (MAR_{BSi}) at IODP Site U1456, as well as (a) relative sea level (Bintanja et al., 2005), (b) insolation calculated at 15°N in June (Berger & Loutre, 1991), (c) Indian summer monsoon index of the Heqing Basin (An et al., 2011), and (d) $\delta^{18}O$ value of seawater from Core NGHP 17 (Gebregiorgis et al., 2018). MIS = marine isotope stage. OC = organic carbon. Note the unique values of almost all of the proxies during sea-level lowstands (gray bars).
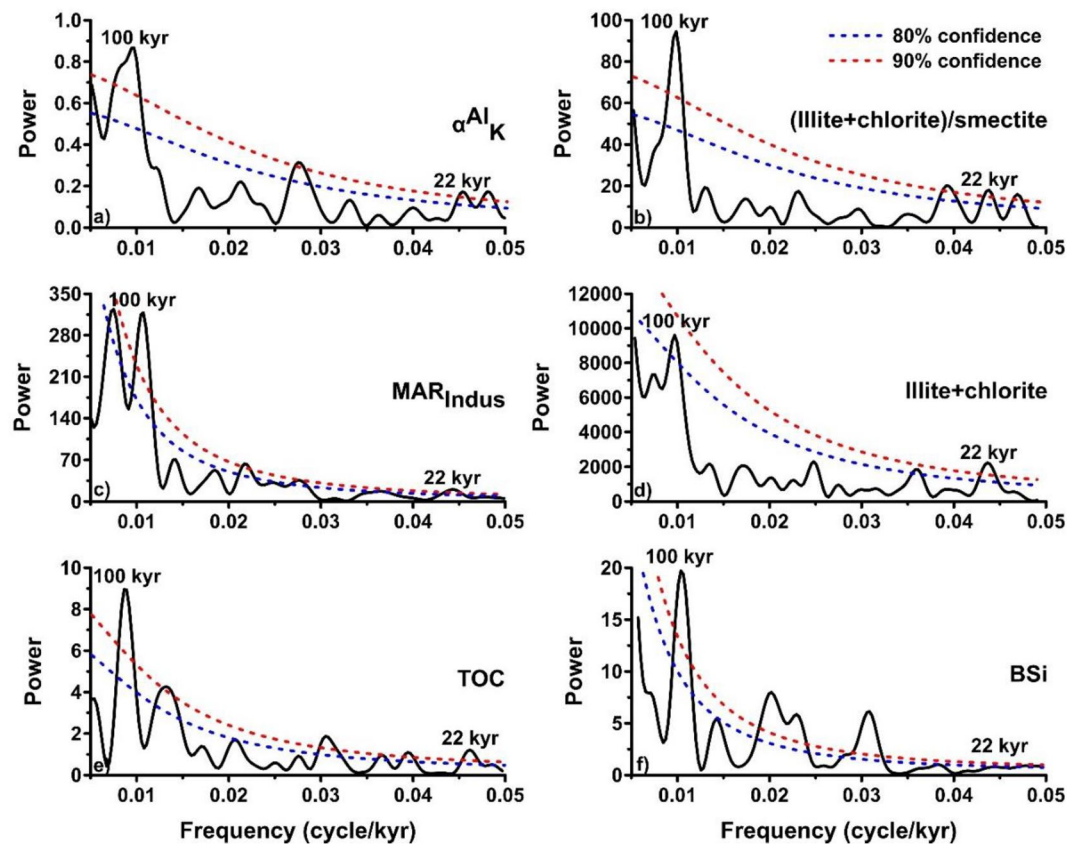
Figure 3. Frequency analyses of some typical proxies at IODP Site U1456, showing the primary orbital periodicities (eccentricity of 100 kyr and precession of 22 kyr) since ~700 ka (Cai et al., 2018, 2019; Chen, Xu et al., 2019, 2020). $\alpha^{Al}_K = (Al/K)_{sample}/(Al/K)_{upper\ continental\ crust}$. MAR_{Indus} = mass accumulation rate of the Indus River detritus. TOC = total organic carbon. BSi = biogenic silica.

accumulation rates of total organic carbon and biogenic silica than interglacial samples. In contrast, glacial sediments are associated with lower average values of the $(Al/K)_{sample}/(Al/K)_{upper\ continental\ crust}$ ratio and ϵ_{Nd} than interglacial samples. In particular, the enrichment factors of the (illite + chlorite)/smectite ratio, as well as mass accumulation rates of the Indus River detritus, biogenic silica, and total organic carbon during glacial periods relative to interglacial stages, are as high as 1.3, 2.2, 1.4, and 1.5, respectively (Table 1). In addition, spectral analyses of these proxies usually reveal strong eccentricity (100 kyr) and precession (22 kyr) frequencies (Figure 3). Furthermore, biogenic silica shows the additional obliquity (41 kyr) frequency (Figure 3).

3.2. Representative Reference Sediment Cores

Representative reference sediment cores (Table 2) from the Arabian Sea, Bay of Bengal, and continental slope in the southern South China Sea show higher average values of the (illite + chlorite)/smectite ratio, turbidite frequency, linear sedimentation rate, content of total organic carbon, mass accumulation rates of terrigenous detritus, eolian dust, and total organic carbon, as well as ratio of total organic carbon to total nitrogen, during glacial periods relative to interglacial periods (Figure 4; Table 3), similar to those at Site U1456 (Figure 2; Table 1). In particular, the enrichment factors of the (illite + chlorite)/smectite ratio, turbidite frequency, content of total organic carbon, as well as mass accumulation rates of eolian dust and total organic carbon during glacial periods relative to interglacial stages are as high as 1.4–2.5, 2.1–5.1, 2.0, 2.1, and 1.8, respectively (Table 3). However, the abyssal South China Sea is characterized by limited increases in the average values of the (illite + chlorite)/smectite ratio, $(Al/K)_{sample}/(Al/K)_{upper\ continental\ crust}$ ratio, and mass accumulation rate of total organic carbon during sea-level lowstands (Figure 4; Table 3).
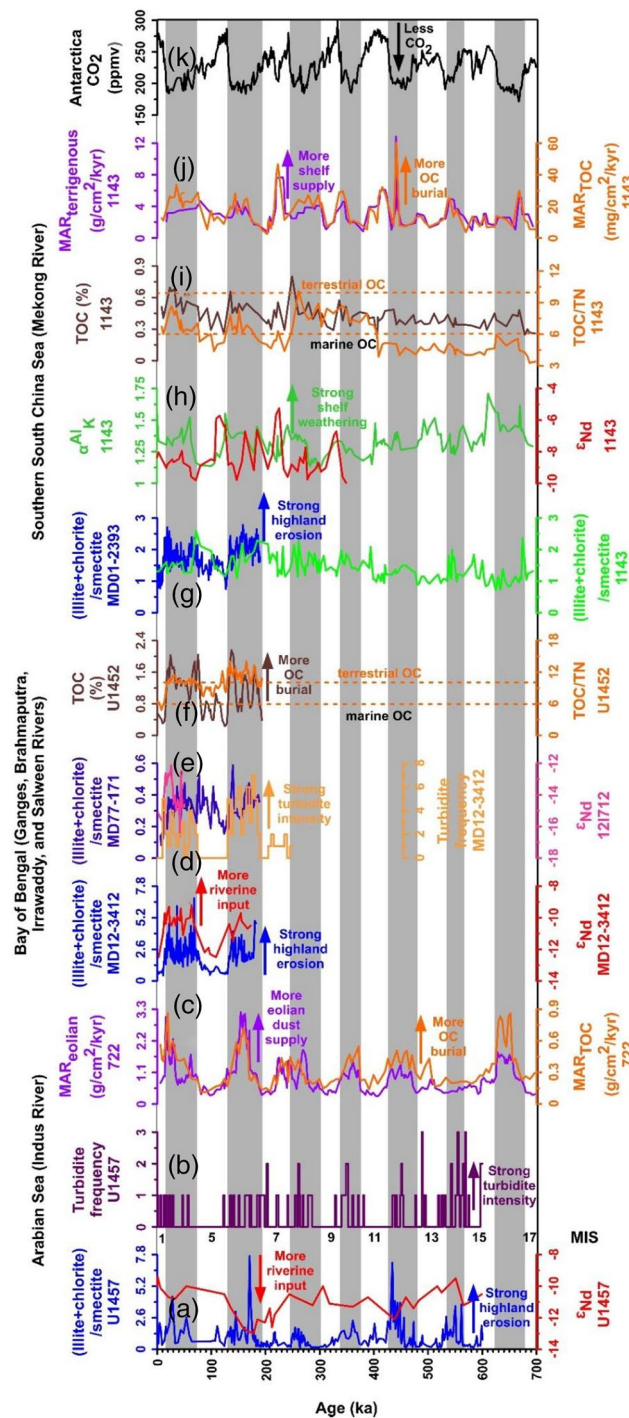
Figure 4. Comparison among (a) physical erosion in the Himalaya and Tibetan Plateau and the produced detritus supply (Yu et al., 2019), (b) turbidite frequency (Yu et al., 2019), and (c) mass accumulation rates of eolian dust (MAR_{eolian}) and total organic carbon (MAR_{TOC}; Clemens et al., 1996) in the deep Arabian Sea; (d) and (e) physical erosion in the Himalaya and Tibetan Plateau and the produced detrital input (Joussain et al., 2016; Liu et al., 2019; Yu et al., 2020), (e) turbidite frequency (Fauquembergue et al., 2019), and (f) content of total organic carbon (TOC) and ratio of total organic carbon to total nitrogen (TOC/TN; Weber et al., 2018) in the abyssal Bay of Bengal; (g) physical erosion in the Himalaya and Tibetan Plateau and on the continental shelf (Liu et al., 2004; Wan et al., 2017), (h) and (i) chemical weathering on the continental shelf and supplies of the produced detritus and organic carbon, respectively (Wan et al., 2017; Wang et al., 2005), (j) mass accumulation rate of terrigenous detritus ($MAR_{terrigenous}$; Wan et al., 2017), and (i) and (j) deposition of organic carbon in the distal southern South China Sea since ~400 ka (Wang et al., 2005); and (k) atmospheric CO_2 concentration from the Antarctic Dome C ice cores (Luthi et al., 2008). MIS = marine isotope stage. $\alpha^{Al}_K = (Al/K)_{sample}/(Al/K)_{upper\ continental\ crust}$. Note the unique values of almost all of the proxies during sea-level lowstands (gray bars).
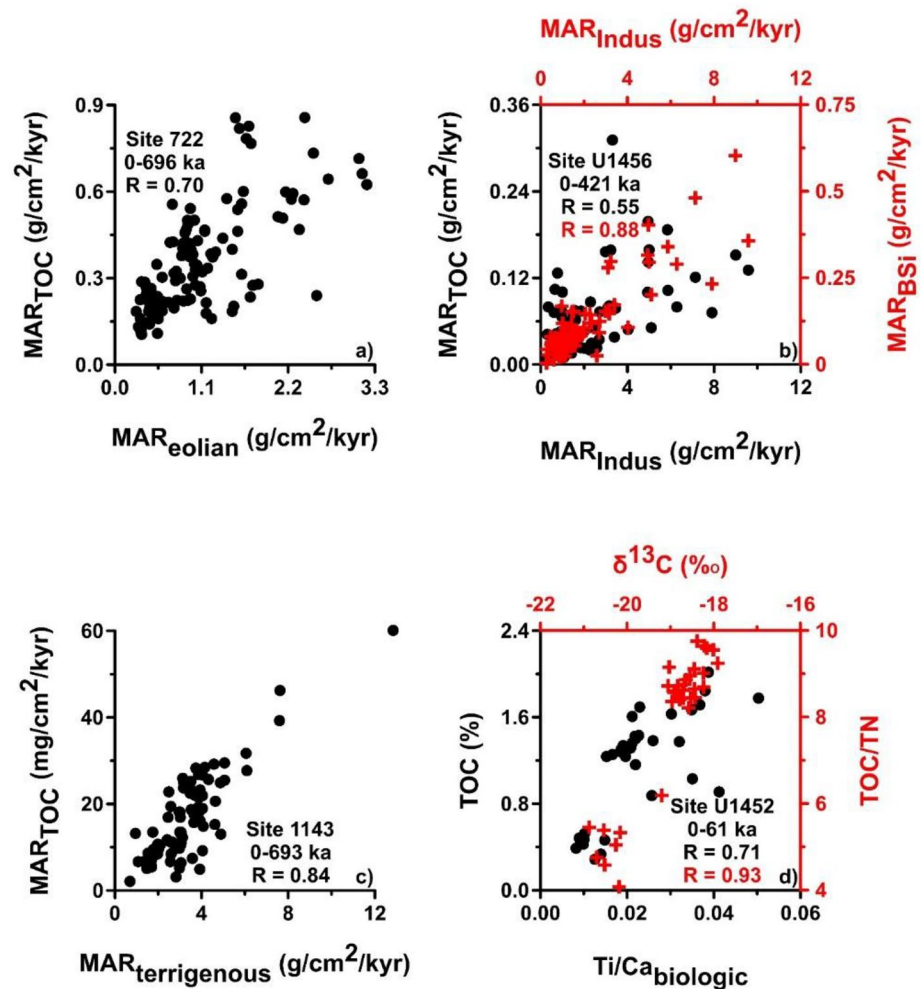
Figure 5. Cross plots of some typical proxies from the representative sediment cores in the study area. R = correlation coefficient. MAR_{eolian} = mass accumulation rate of eolian dust. MAR_{TOC} = mass accumulation rate of total organic carbon. MAR_{Indus} = mass accumulation rate of the Indus River detritus. MAR_{BSi} = mass accumulation rate of biogenic silica. $MAR_{terrigenous}$ = mass accumulation rate of terrigenous detritus. $Ti/Ca_{biologic}$ = ratio of Ti to biologic Ca. TOC = total organic carbon. TOC/TN = ratio of total organic carbon to total nitrogen.

3.3. Correlations Between Typical Proxies in the Study Sediment Cores

The cross plots of typical proxies (Figure 5), including the terrigenous detritus supply from the Himalaya and Tibetan Plateau (mass accumulation rates of the Indus River detritus and ratio of Ti to biologic Ca), eolian dust contribution from Somali and Arabia (mass accumulation rate of eolian dust), terrestrial detritus input from the continental shelf in the southern South China Sea (mass accumulation rate of terrigenous detritus), sea surface productivity (mass accumulation rate of biogenic silica), and the source (ratio of total organic carbon to total nitrogen and $\delta^{13}C$ value of organic matter) and burial (content and mass accumulation rate of total organic carbon) of organic carbon, in selected marine sediment cores indicate the close correlations between terrestrial detritus input and organic carbon preservation in the distal tropical Arabian Sea, Bay of Bengal, and southern South China Sea during the Quaternary.

4. Discussion

Based on clay mineralogy, elemental geochemistry, and Sr-Nd isotopic compositions, the detrital sediments deposited at IODP Site U1456 since ~700 ka have been deduced to originate mainly from the Indus River, especially during sea-level lowstands (Chen, Xu et al., 2019, 2020). Increases in average values of

the (illite + chlorite)/smectite ratio and $^{87}Sr/^{86}Sr$ ratio and decreases in average values of the $(Al/K)_{sample}/(Al/K)_{upper\ continental\ crust}$ ratio and ε_{Nd} at the site during glacial periods indicate a strong enhancement of physical erosion in the Himalayan and Tibetan highlands and large inputs of the produced terrigenous detritus into the eastern Arabian Sea (Figure 2; Table 1), dominantly driven by sea-level lowstands and, thus, activation of deep-sea channels (Chen, Xu et al., 2019, 2020; Yu et al., 2019). In addition, our records show that the Indian summer monsoon intensity may play an important role in modulating the physical erosion and chemical weathering processes with respect to the precession (22 kyr) periodicity (Figure 3; Chen, Xu, et al., 2019, 2020; Hein et al., 2020). During glacial periods with relatively low sea level and weak Indian summer monsoon intensity, interestingly, the increased highland erosion (high average (illite + chlorite)/smectite ratio), activation of deep-sea channels (enhanced average turbidite frequency; Figure 4; Yu et al., 2019), and strengthened supply of terrestrial detritus (high average mass accumulation rate of the Indus River detritus) to the site are associated with prominent enhancements in average mass accumulation rates of biogenic silica and total organic carbon and increases in the ratio of total organic carbon to total nitrogen (Figure 2; Table 1). This association reveals the stimulated marine productivity and increased influence of organic matter with terrigenous origin (ratio of total organic carbon to total nitrogen much higher than 6; Lim et al., 2011; Lee et al., 2020; Rixen et al., 2019; Xu et al., 2020). The opposite phase occurs during interglacial periods (Figure 2; Table 1), with the exception of anomalous values in marine isotope stage 13, possibly resulting from a continental erosion event or variations in marine circulation (Chen et al., 2020; Ziegler et al., 2010).

Similar dramatic fluctuations in highland erosion and inputs of terrestrial detritus and organic matter into the sea during the Quaternary over orbital timescales have been frequently found in many nearby sediment cores (e.g., correlation coefficient of 0.71, $p < 0.05$, between the ratio of Ti to biologic Ca and content of total organic carbon at Site U1452 since 61 ka; Figure 5; Weber et al., 2018) from the distal eastern Arabian Sea and Bay of Bengal (Figure 4; Table 3), which are characterized by significant contributions from the Himalaya and Tibetan Plateau (Joussain et al., 2016; Liu et al., 2019; Yu et al., 2019, 2020). This result indicates the generally common nature of the abovementioned phenomena in the seas during the Quaternary over orbital timescales. Furthermore, the strong correlation between the mass accumulation rate of eolian dust, originating from physical erosion in Somali and Arabia, and mass accumulation rate of total organic carbon at ODP Site 722 (Figure 5; correlation coefficient of 0.70, $p < 0.05$) indicates remarkable increases in the contributions of terrigenous detritus and burial of organic carbon in the distal western Arabian Sea during glacial periods (Figure 4; Table 3; Clemens et al., 1996). Similarly, biogenic silica productivity likely increased in the Bay of Bengal during glacial and stadial stages, indicative of the enhanced Indian winter monsoon intensity and eolian matter supply on the obliquity (41 kyr) frequency, potentially associated with sea-level lowstands and/or the higher influence of the Northern Hemisphere westerlies on the dust transport from the Himalaya and Tibetan Plateau (Weber et al., 2018).

Such a glaciation-associated enhancement in Himalayan and Tibetan erosion and supplies of the produced materials to the tropical marginal seas is evident in sediment cores from the continental slope in the southern South China Sea (Figure 4; Table 3; Liu et al., 2004). However, this covariation among proxies for the highland erosion and associated transport of terrigenous detritus and organic matter during the Quaternary over orbital timescales is not found in the abyssal southern South China Sea (Figures 4 and 5; Table 3; Wan et al., 2017; Wang et al., 2005). In contrast, the enhanced weathering of Mekong-derived silicates on the exposed continental shelf and increased terrestrial organic carbon input are typical features in this deep sea during sea-level lowstands since ~400 ka, with the exception of the potential influences of marine isotope stage 13 and mid-Brunhes events (Figure 4; Table 3; Chen et al., 2020; Wan et al., 2017; Wang et al., 2005; Ziegler et al., 2010). Conclusively, all these results emphasize the significant influence of terrigenous detritus and organic carbon supplies, closely associated with highland erosion and continental shelf weathering, on the distal eastern Arabian Sea (e.g., correlation coefficient of 0.55, $p < 0.05$, between mass accumulation rates of the Indus River detritus and total organic carbon at Site U1456 since ~700 ka), Bay of Bengal (e.g., correlation coefficient of 0.71, $p < 0.05$, between the ratio of Ti to biologic Ca and content of total organic carbon at Site U1452 since 61 ka; Weber et al., 2018), and southern South China Sea (e.g., correlation coefficient of 0.84, $p < 0.05$, between mass accumulation rates of terrigenous detritus and total organic carbon at Site 1143 since ~700 ka; Wan et al., 2017; Wang et al., 2005) during the Quaternary glacial periods (Figures 2, 4, and 5; Tables 1–3).

The tropical seas may have played an important role in modulating global climate during the Quaternary through several different mechanisms (e.g., Beaufort et al., 2001; Jacobel et al., 2017; Wan et al., 2017; Winckler et al., 2016; Xu et al., 2018, 2020). In the study area, terrigenous organic carbon burial in the sea associated with physical erosion in the Himalayan and Tibetan highlands and chemical weathering in the Himalayan and Tibetan lowlands have often been assumed to be the two dominant processes involved in buffering the atmospheric CO_2 concentration and climate during the Neogene, although the relative importance of each mechanism is still under debate (France-Lanord & Derry, 1997; Galy et al., 2007; Hein et al., 2020; Wan et al., 2017). By combining previous results and new data on sedimentary source and sink processes in the study area (Tables 1–3), we assess how these processes have controlled inputs of terrestrial detritus, nutrients, and organic matter, marine productivity, and organic carbon burial and evaluate their significance with respect to the Quaternary carbon cycle and climate variation.

4.1. Physical Erosion in the Himalaya and Tibetan Plateau and the Organic Carbon Burial

During glacial periods, the cold and dry climate, mountain glacier advance, reworking of continental shelf sediments originating from the Himalaya and Tibetan Plateau during interglacial periods, and activation of deep-sea channels occurred (An et al., 2011; Fauquembergue et al., 2019). They resulted in strengthened highland erosion; increased supplies of riverine detritus, nutrients (e.g., Si), and organic matter; and enhanced marine productivity in the distal Arabian Sea (e.g., correlation coefficient of 0.88, $p < 0.05$, between mass accumulation rates of the Indus River detritus and biogenic silica at Site U1456 since ~700 ka) and Bay of Bengal (Cartapanis et al., 2016; Lee et al., 2020; Sirocko et al., 2000; Weber et al., 2018; Yu et al., 2020). Correspondingly, the average values of the (illite + chlorite)/smectite ratio, turbidite frequency, mass accumulation rates of terrigenous detritus, biogenic silica, and total organic carbon, and ratio of total organic carbon to total nitrogen all increased in the seas during sea-level lowstands (Figures 2, 4, and 6; Tables 1–3). In addition, the relatively strong intensity of the Indian winter monsoon at the time may have led to enhanced inputs of eolian dust and associated organic matter (e.g., correlation coefficient of 0.70, $p < 0.05$, between mass accumulation rates of eolian dust and total organic carbon at Site 722 since ~700 ka; Figure 5; Clemens et al., 1996), thereby stimulating marine productivity and organic carbon burial through eolian nutrient supply (e.g., Fe) or shoaling of the thermocline in the seas (Fontugne & Duplessy, 1986; Moffett & German, 2020; Sirocko et al., 2000; Weber et al., 2018).

The strengthened terrigenous inputs of detritus, nutrients, and organic carbon, stimulated marine productivity levels, persistent existence of the oxygen minimum zone, high sedimentation rates, and reduced oxygen exposure of terrestrial matter in the seas during glacial periods accounted for the significant enhancement in the preservation of organic carbon (Cartapanis et al., 2016; Jaccard & Galbraith, 2012; Kim et al., 2018; Weber et al., 2018; Ziegler et al., 2010), averaging 2.1 and 2.8 times higher than those at 0.5 ka (core top sediments; Figures 2 and 4; Tables 1–3). These amounts are significantly higher than the increases in the global deep-sea mass accumulation rate of total organic carbon during the Last Glacial Maximum to the Holocene (1.5 times; Cartapanis et al., 2016) and during late marine isotope stage 6 to marine isotope stage 5e (1.6 times; Cartapanis et al., 2016). Combining an average net growth (burial > weathering) of the sedimentary organic carbon reservoir in the Bay of Bengal (0.58×10^{12} mol/yr) during the Neogene (France-Lanord & Derry, 1997), we can preliminarily deduce that this burial flux may have been as high as ~0.85×10^{12} mol/yr during the Quaternary sea-level lowstands, accounting for ~5% (~4 ppmv) of the glacial decrease in the atmospheric CO_2 concentration (~80 ppmv; Luthi et al., 2008). Similarly, we preliminarily estimate an average burial flux of organic carbon in the eastern Arabian Sea during glacial periods to be ~0.20×10^{12} mol/yr, based on its source region, climate, marine environment, turbidite activity, and total organic carbon content at the core top (~0.5%) that are generally similar to those for the Bay of Bengal, as well as the ratio of the average mass accumulation rate of total organic carbon during glacial periods to that during interglacial periods and the annual fluvial sediment discharges of major rivers for the seas (Figures 1, 2, and 4; Tables 1–3; An et al., 2011; Fauquembergue et al., 2019; Joussain et al., 2016; Liu et al., 2019, 2020; Milliman & Farnsworth, 2011; Rixen et al., 2019; Weber et al., 2018; Yu et al., 2019). This burial flux is equivalent to ~1% (~1 ppmv) of the decrease in the atmospheric CO_2 concentration during sea-level lowstands (~80 ppmv; Luthi et al., 2008). Therefore, the Bay of Bengal and eastern Arabian Sea may act as an important sink (~1.05×10^{12} mol/yr) of organic carbon during the Quaternary glacial
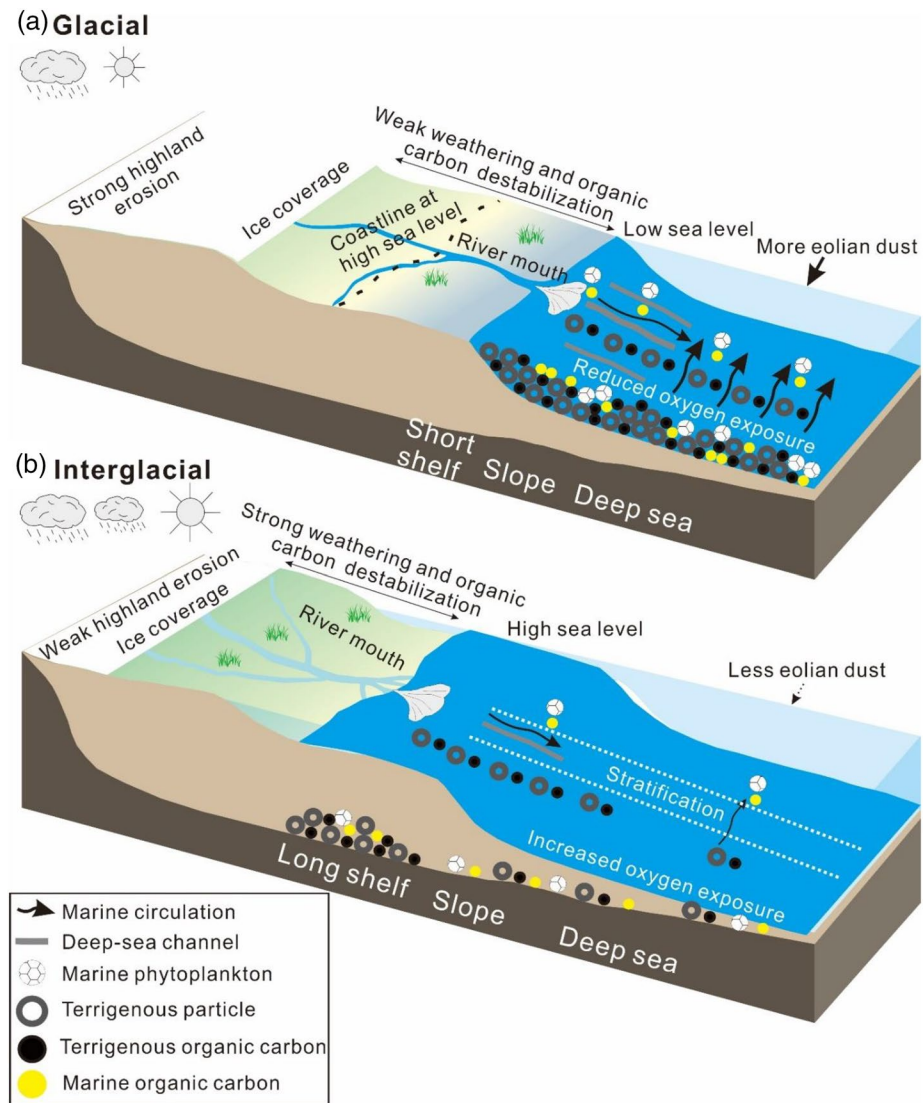
Figure 6. Schematic model of processes associated with physical erosion in the Himalaya and Tibetan Plateau and transport of the produced detritus and organic matter, eolian dust input, hydrological dynamics, marine productivity, and organic carbon burial in the Arabian Sea and Bay of Bengal during (a) glacial and (b) interglacial periods, derived from both the current study and previous research (e.g., An et al., 2011; Chen et al., 2019a 2019b; Clemens et al., 1996; Fauquembergue et al., 2019; Hein et al., 2020; Kim et al., 2018; Lee et al., 2020; Liu et al., 2019; Ramaswamy et al., 2008; Weber et al., 2018; Yu et al., 2019).

periods, thereby contributing ~6% (~5 ppmv) of the decrease in the atmospheric CO_2 concentration during these times (~80 ppmv; Luthi et al., 2008). During interglacial periods excluding marine isotope stage 13 (which possibly resulted from a continental erosion event or variations in marine circulation; Chen et al., 2020; Ziegler et al., 2010), the opposite phase may occur in the continental source regions and sedimentary seas (Figures 2, 4, and 6; Tables 1–3; An et al., 2011; Chen, Xu, et al., 2019, 2020; Clemens et al., 1996; Fauquembergue et al., 2019; Li et al., 2018; Liu et al., 2019, 2020; Ramaswamy et al., 2008; Rixen et al., 2019; Weber et al., 2018; Yu et al., 2019, 2020). Similar changes in terrigenous detritus and organic matter supplies, marine productivity, sedimentation rates, and redox conditions of the bottom water, together with the forcing mechanisms, in the tropical marginal seas surrounding southeast Asia during the Quaternary were reported (Beaufort et al., 2001; Chen, Luo, et al., 2019; Xiong et al., 2018; Xu et al, 2018, 2020), suggesting the generally common nature of the abovementioned phenomena.

4.2. Chemical Weathering of Himalayan and Tibetan Silicates on the Continental Shelf and the Organic Carbon Burial

The glacial-interglacial fluctuations in highland erosion and associated terrestrial input during the Quaternary are also evident in sediment cores collected off the Mekong River mouth on the continental slope in the southern South China Sea (Figure 4; Tables 2 and 3; Colin et al., 2010; Liu et al., 2004). In addition, the extensive exposure of unconsolidated silicate sediments, dominantly originating from the Mekong River, on the tropical continental shelf in southeast Asia during sea-level lowstands was important for enhanced shelf weathering and terrigenous organic carbon supply to the abyssal southern South China Sea (Wan et al., 2017; Wang et al., 2005). This conclusion is supported by increases in average values of the $(Al/K)_{sample}/(Al/K)_{upper\ continental\ crust}$ ratio, mass accumulation rate of total organic carbon, and ratio of total organic carbon to total nitrogen at ODP Site 1143 during glacial periods since ~400 ka (Figure 4; Table 3; Wan et al., 2017; Wang et al., 2005). Quantitatively, the average mass accumulation rate of total organic carbon at the site during sea-level lowstands was 1.6 times higher than that for the core top sediment deposited during the late Holocene (Figure 4; Tables 2 and 3; Wang et al., 2005). This value is equivalent to the increases in the global deep-sea mass accumulation rate of total organic carbon during the Last Glacial Maximum to the Holocene (1.5 times; Cartapanis et al., 2016) and during late marine isotope stage 6 to marine isotope stage 5e (1.6 times; Cartapanis et al., 2016). The increased silicate weathering on the exposed tropical continental shelves, including that in the South China Sea, may account for an average of ~9% (~7 ppmv) of the observed decrease in the atmospheric CO_2 concentration during glacial periods (~80 ppmv; Luthi et al., 2008; Wan et al., 2017). Furthermore, the sedimentary organic carbon reservoir in the southern South China Sea during sea-level lowstands may have an average value of $\sim 0.07 \times 10^{12}$ mol/yr, estimated on the basis of the abovementioned calculation method for the eastern Arabian Sea, its ratio of the average mass accumulation rate of total organic carbon during glacial periods to that during interglacial periods, its total organic carbon content at the core top (~0.5%) that is generally similar to those for the Bay of Bengal and eastern Arabian Sea, and the annual fluvial sediment discharges of major rivers for the seas (Figures 1, 2, and 4; Wang et al., 2005; Milliman & Farnsworth, 2011; Weber et al., 2018). This burial flux corresponds to ~0.5% (~0.4 ppmv) of the decrease in the atmospheric CO_2 concentration during glacial periods (~80 ppmv; Luthi et al., 2008).

4.3. Significance of Tropical Regions in Modulating the Atmospheric CO₂ Level

Continental surface weathering and erosion can affect the long-term ocean-atmosphere budget of CO_2 both through the consumption of carbonic acid during silicate weathering and the associated burial of organic carbon in the sea, especially in tropical regions (France-Lanord & Derry, 1997; Galy et al., 2007; Hilton & West, 2020; Wan et al., 2017; Xu et al, 2018, 2020). From the abovementioned discussion, we can conclude that strengthened physical erosion in the Himalayan and Tibetan highlands, increased chemical weathering of silicates (dominantly originating from the mountains) on the exposed tropical continental shelf in southeast Asia, activation of deep-sea channels, stimulated marine productivity, and large-scale burial of organic carbon with both terrestrial and marine origins during the Quaternary glacial periods made the distal Arabian Sea, Bay of Bengal, and southern South China Sea important contributors to the modulation of global organic carbon preservation and the atmospheric CO_2 concentration, together accounting for ~1/4 of the current global marine burial flux ($\sim 1.12 \times 10^{12}$ mol/yr; France-Lanord & Derry, 1997; Wang et al., 2005; Galy et al., 2007; Cartapanis et al., 2016). The burial flux in the study area is equivalent to ~7% (~6 ppmv) of the decrease in the atmospheric CO_2 concentration during sea-level lowstands (~80 ppmv; Luthi et al., 2008). However, such deductions should be further confirmed with multiproxy measurements, especially in quantitative terms, on additional sediment cores in these seas.

In addition, the tropical regions may have played an important role in modulating the global climate during glacial periods through the enhanced silicate weathering on the exposed tropical continental shelves (Wan et al., 2017) and the increased silicate weathering in the tropical volcanic arcs (Xu et al., 2018, 2020). These processes account for ~9% (~7 ppmv) and ~10% (~8 ppmv), respectively, of the decrease in the atmospheric CO_2 concentration during sea-level lowstands (~80 ppmv; Luthi et al., 2008). The results highlight that tropical regions were an important contributor (~1/4) to the decrease in the atmospheric CO_2 concentration during glacial periods.

Along with the increasingly severe anthropogenic activity and the associated high rates of physical erosion and chemical weathering in the Himalayan and Tibetan highlands, mass accumulation rates of total organic carbon in tropical marginal seas surrounding the mountains are likely to increase, thereby decreasing the atmospheric CO_2 concentration and buffering global warming. The current study, therefore, may facilitate better understanding and projections of carbon and climate cycles in the future.

5. Conclusions

For the first time, comprehensive reconstructions of various proxies, including continental surface erosion and weathering, terrigenous supply, marine productivity, and burial of organic carbon, in 13 representative sediment cores were acquired and compiled for the distal tropical Arabian Sea, Bay of Bengal, and southern South China Sea to quantitatively assess their significance for the Quaternary organic carbon and climate variations over orbital timescales. The enhanced Himalayan and Tibetan highland erosion during glacial periods resulted in increased terrestrial sediment supplies through major rivers and eolian dust, stimulated marine productivity, and abundant burial of the produced terrigenous detritus and organic carbon with both terrestrial and marine origins in the deep Arabian Sea and Bay of Bengal and on the continental slope in the southern South China Sea. In contrast, chemical weathering of the Himalaya- and Tibet-derived silicates on the continental shelf may have modulated the preservation of organic carbon in the abyssal southern South China Sea over orbital timescales. The consistent enhancements in organic carbon burial in the seas during sea-level lowstands, averaging 1.6–2.8 times greater than those during the late Holocene, represented an important sink ($\sim 1.12 \times 10^{12}$ mol/yr) for the global organic matter storage and, thus, a non-negligible contributor ($\sim 7\%$; ~ 6 ppmv) to the decrease in the atmospheric CO_2 concentration at these times. Pending further research on the more detailed quantitative estimates of organic carbon source and flux, the current results, together with those reported in our recent studies (Wan et al., 2017; Xu et al., 2018, 2020), effectively demonstrate the unique significance of tropical regions in modulating the atmospheric CO_2 ($\sim 1/4$ of the total decrease) and thus partly explain the global cooling during glacial periods.

Data Availability Statement

The data generated by this study are available in the Pangaea database (https://doi.pangaea.de/10.1594/PANGAEA.920935).

References

An, Z. S., Clemens, S. C., Shen, J., Qiang, X. K., Jin, Z. D., Sun, Y. B., et al. (2011). Glacial-interglacial Indian summer monsoon dynamics. *Science*, *333*(6043), 719–723. https://doi.org/10.1126/science.1203752

Baronas, J. J., Stevenson, E. I., Hackney, C. R., Darby, S. E., Bickle, M. J., Hilton, R. G., et al. (2020). Integrating suspended sediment flux in large alluvial river channels: Application of a synoptic Rouse based model for the Irrawaddy and Salween rivers. *Journal of Geophysical Research: Earth Surface*, *125*(9), e2020JF005554. https://doi.org/10.1029/2020JF005554

Beaufort, L., de Garidel-Thoron, T., Mix, A. C., & Pisias, N. G. (2001). ENSO-like forcing on oceanic primary production during the late Pleistocene. *Science*, *293*(5539), 2440–2444. https://doi.org/10.1126/science.293.5539.2440

Berger, A., & Loutre, M. F. (1991). Insolation values for the climate of the last 10 million years. *Quaternary Sciences Review*, *10*, 297–317. https://doi.org/10.1016/0277-3791(91)90033-Q

Bianchi, T. S., & Allison, M. A. (2009). Large-river delta-front estuaries as natural "recorders" of global environmental change. *Proceedings of the National Academy of Sciences of the United States of America*, *106*(20), 8085–8092. https://doi.org/10.1073/pnas.0812878106

Bintanja, R., van de Wal, R. S., & Oerlemans, J. (2005). Modelled atmospheric temperatures and global sea levels over the past million years. *Nature*, *437*(7055), 125–128. https://doi.org/10.1038/nature03975

Blair, N. E., & Aller, R. C. (2012). The fate of terrestrial organic carbon in the marine environment. *Annual Review of Marine Science*, *4*(1), 401–423. https://doi.org/10.1146/annurev-marine-120709-142717

Blattmann, T. M., Liu, Z. F., Zhang, Y., Zhao, Y. L., Haghipour, N., Montluçon, D. B., et al. (2019). Mineralogical control on the fate of continentally derived organic matter in the ocean. *Science*, *366*(6466), 742–745. https://doi.org/10.1126/science.aax5345

Burdige, D. J. (2005). Burial of terrestrial organic matter in marine sediments: A re-assessment. *Global Biogeochemical Cycles*, *19*(4), GB4011. https://doi.org/10.1029/2004GB002368

Cai, M. J., Xu, Z. K., Clift, P. D., Khim, B.-K., Lim, D. I., Yu, Z. J., et al. (2018). Long-term history of sediment inputs to the eastern Arabian Sea and its implications for the evolution of the Indian summer monsoon since 3.7 Ma. *Geological Magazine*, *157*(6), 908–919. https://doi.org/10.1017/S0016756818000857

Cai, M. J., Xu, Z. K., Clift, P. D., Lim, D. I., Khim, B.-K., Yu, Z. J., et al. (2019). Depositional history and Indian summer monsoon controls on the silicate weathering of sediment transported to the eastern Arabian Sea: Geochemical records from IODP Site U1456 since 3.8 Ma. *Geochemistry, Geophysics, Geosystems*, *20*(9), 4336–4353. https://doi.org/10.1029/2018GC008157

Cartapanis, O., Bianchi, D., Jaccard, S. L., & Galbraith, E. D. (2016). Global pulses of organic carbon burial in deep-sea sediments during glacial maxima. *Nature Communications*, *7*, 10796. https://doi.org/10.1038/ncomms10796

Chen, H. J., Xu, Z. K., Clift, P. D., Lim, D. I., Khim, B.-K., & Yu, Z. J. (2019). Orbital-scale evolution of the Indian summer monsoon since 1.2 Ma: Evidence from clay mineral records at IODP Expedition 355 Site U1456 in the eastern Arabian Sea. *Journal of Asian Earth Sciences*, *174*, 11–22. https://doi.org/10.1016/j.jseaes.2018.10.012

Chen, H. J., Xu, Z. K., Lim, D. I., Clift, P. D., Chang, F. M., Li, T. G., et al. (2020). Geochemical records of the provenance and silicate weathering/erosion from the eastern Arabian Sea and their responses to the Indian summer monsoon since the Mid-Pleistocene. *Paleoceanography and Paleoclimatology*, *35*, e2019PA003732. https://doi.org/10.1029/2019PA003732

Chen, L. Y., Luo, M., Dale, A. W., Rashid, H., Lin, G., & Chen, D. F. (2019). Reconstructing organic matter sources and rain rates in the southern West Pacific Warm Pool during the transition from the deglaciation period to early Holocene. *Chemical Geology*, *529*, 119291. https://doi.org/10.1016/j.chemgeo.2019.119291

Clemens, S. C., Murray, D. W., & Prell, W. L. (1996). Nonstationary phase of the Plio-Pleistocene Asian monsoon. *Science*, *274*(5289), 943–948. https://doi.org/10.1126/science.274.5289.943

Colin, C., Siani, G., Sicre, M.-A., & Liu, Z. F. (2010). Impact of the East Asian monsoon rainfall changes on the erosion of the Mekong River basin over the past 25,000 yr. *Marine Geology*, *271*(1–2), 84–92. https://doi.org/10.1016/j.margeo.2010.01.013

Colin, C., Turpin, L., Bertaux, J., Desprairies, A., & Kissel, C. (1999). Erosional history of the Himalayan and Burman ranges during the last two glacial-interglacial cycles. *Earth and Planetary Science Letters*, *171*(4), 647–660. https://doi.org/10.1016/S0012-821X(99)00184-3

Colin, C., Turpin, L., Blamart, D., Frank, N., Kissel, C., & Duchamp, S. (2006). Evolution of weathering patterns in the Himalayas and Indo-Burman ranges over the last 280 kyr: Effects of sediment provenance on ^{87}Sr/^{86}Sr ratios tracers. *Geochemistry, Geophysics, Geosystems*, *7*(3), Q03007. https://doi.org/10.1029/2005GC000962

D´Asaro, E., Altabet, M., Kumar, N. S., & Ravichandran, M. (2020). Structure of the Bay of Bengal oxygen deficient zone. *Deep-Sea Research Part II*, *179*, 104650. https://doi.org/10.1016/j.dsr2.2019.104650

Fauquembergue, K., Fournier, L., Zaragosi, S., Bassinot, F., Kissel, C., Malaizé, B., et al. (2019). Factors controlling frequency of turbidites in the Bengal fan during the last 248 kyr cal BP: Clues from a presently inactive channel. *Marine Geology, 415, 105965.* https://doi.org/10.1016/j.margeo.2019.105965

Fontugne, M. R., & Duplessy, J.-C. (1986). Variations of the monsoon regime during the upper quaternary: Evidence from carbon isotopic record of organic matter in North Indian Ocean sediment cores. *Palaeogeography, Palaeoclimatology, Palaeoecology*, *56*(1–2), 69–88. https://doi.org/10.1016/0031-0182(86)90108-2

France-Lanord, C., & Derry, L. A. (1997). Organic carbon burial forcing of the carbon cycle from Himalayan erosion. *Nature*, *390*(6655), 65–67. https://doi.org/10.1038/36324

Galy, V., France-Lanord, C., Beysac, O., Faure, P., Kudrass, H., & Palho, F. (2007). Efficient organic carbon burial in the Bengal fan sustained by the Himalayan erosional system. *Nature*, *450*(7168), 407–410. https://doi.org/10.1038/nature06273

Gebregiorgis, D., Hathorne, E. C., Giosan, L., Clemens, S. C., Nurnberg, D., & Frank, M. (2018). Southern Hemisphere forcing of South Asian monsoon precipitation over the past ~1 million years. *Nature Communications*, *9*, 4702. https://doi.org/10.1038/s41467-018-07076-2

Hein, C. J., Usman, M., Eglinton, T. I., Haghipour, N., & Galy, V. (2020). Millennial-scale hydroclimate control of tropical soil carbon storage. *Nature*, *581*(7806), 63–66. https://doi.org/10.1038/s41586-020-2233-9

Hilton, R. G. (2017). Climate regulates the erosional carbon export from the terrestrial biosphere. *Geomorphology*, *277*, 118–132. http://dx.doi.org/10.1016/j.geomorph.2016.03.028

Hilton, R. G., & West, A. J. (2020). Mountains, erosion and the carbon cycle. *Nature Reviews Earth & Environment*, *1*, 284–299. https://doi.org/10.1038/s43017-020-0058-6

Jaccard, S. L., & Galbraith, E. D. (2012). Large climate-driven changes of oceanic oxygen concentrations during the last deglaciation. *Nature Geoscience*, *5*(2), 151–156. https://doi.org/10.1038/NGEO1352

Jacobel, A. W., McManus, J. F., Anderson, R. F., & Winckler, G. (2017). Repeated storage of respired carbon in the equatorial Pacific Ocean over the last three glacial cycles. *Nature Communications*, *8*, 1727. https://doi.org/10.1038/s41467-017-01938-x

Joussain, R., Colin, C., Liu, Z. F., Meynadier, L., Fournier, L., Fauquembergue, K., et al. (2016). Climatic control of sediment transport from the Himalayas to the proximal NE Bengal Fan during the last glacial-interglacial cycle. *Quaternary Science Reviews*, *148*, 1–16. http://dx.doi.org/10.1016/j.quascirev.2016.06.016

Khim, B.-K., Horikawa, K., Asahara, Y., Kim, J.-E., & Ikehara, M. (2018). Detrital Sr-Nd isotopes, sediment provenances and depositional processes in the Laxmi Basin of the Arabian Sea during the last 800 ka. *Geological Magazine*, *157*(6), 895–907. https://doi.org/10.1017/S0016756818000596

Kim, J.-E., Khim, B.-K., Ikehara, M., & Lee, J. (2018). Orbital-scale denitrification changes in the Eastern Arabian Sea during the last 800 kyrs. *Scientific Reports*, *8*, 7027. https://doi.org/10.1038/s41598-018-25415-7

Lee, J., Kim, S., & Khim, B.-K. (2020). A paleoproductivity shift in the northwestern Bay of Bengal (IODP Site U1445) across the Mid-Pleistocene transition in response to weakening of the Indian summer monsoon. *Palaeogeography, Palaeoclimatology, Palaeoecology*, *560*, 110018. https://doi.org/10.1016/j.palaeo.2020.110018

Li, Y. T., Clift, P. D., Böning, P., Blusztajn, J., Murray, R. W., Ireland, T., et al. (2018). Continuous Holocene input of river sediment to the Indus Submarine Canyon. *Marine Geology*, *406*, 159–176. https://doi.org/10.1016/j.margeo.2018.09.011

Lim, D. I., Xu, Z. K., Choi, J. Y., Kim, S. Y., Kim, E. H., Kang, S. R., et al. (2011). Paleoceanographic changes in the Ulleung Basin, East (Japan) Sea, during the last 20,000 years: Evidence from variations in element composition of core sediments. *Progress in Oceanography*, *88*, 101–115. https://doi.org/10.1016/j.pocean.2010.12.016

Liu, J. G., He, W., Cao, L., Zhu, Z., Xiang, R., Li, T. G., et al. (2019). Staged fine-grained sediment supply from the Himalayas to the Bengal Fan in response to climate change over the past 50,000 years. *Quaternary Science Reviews*, *212*, 164–177. https://doi.org/10.1016/j.quascirev.2019.04.008

Liu, J. P., Kuehl, S. A., Pierce, A. C., Williams, J., Blair, N. E., Harris, C., et al. (2020). Fate of Ayeyarwady and Thanlwin Rivers Sediments in the Andaman Sea and Bay of Bengal. *Marine Geology*, *423*, 106137. https://doi.org/10.1016/j.margeo.2020.106137

Liu, Z. F., Colin, C., Trentesaux, A., Blamart, D., Bassinot, F., Siani, G., et al. (2004). Erosional history of the eastern Tibetan Plateau since 190 kyr ago: Clay mineralogical and geochemical investigations from the southwestern South China Sea. *Marine Geology*, *209*, 1–18. https://doi.org/10.1016/j.margeo.2004.06.004

Luthi, D., Floch, M. L., Bereiter, B., Blunier, T., Barnola, J. M., Siegenthaler, U., et al. (2008). High-resolution carbon dioxide concentration record 650,000–800,000 years before present. *Nature*, *453*(7193), 379–382. https://doi.org/10.1038/nature06949

Milliman, J. D., & Farnsworth, K. L. (2011). *River discharge to the coastal ocean: A global synthesis*. Cambridge, UK: Cambridge University Press.

Moffett, J. W., & German, C. R. (2020). Distribution of iron in the Western Indian Ocean and the Eastern tropical South pacific: An inter-basin comparison. *Chemical Geology*, *532*, 119334. https://doi.org/10.1016/j.chemgeo.2019.119334

Pandey, D. K., Clift, P. D., Kulhanek, D. K., & the Expedition 355 Scientists. (2016). Arabian Sea monsoon. In Proceedings of the International Ocean Discovery Program (Vol. 355). College Station, TX: International Ocean Discovery Program. https://doi.org/10.14379/iodp.proc.355.101.2016

Ramaswamy, V., Gaye, B., Shirodkar, P. V., Rao, P. S., Chivas, A. R., Wheeler, D., et al. (2008). Distribution and sources of organic carbon, nitrogen and their isotopic signatures in sediments from the Ayeyarwady (Irrawaddy) continental shelf, northern Andaman Sea. *Marine Chemistry*, *111*, 137–150. https://doi.org/10.1016/j.marchem.2008.04.006

Rixen, T., Gaye, B., & Emeis, K.-C. (2019). The monsoon, carbon fluxes, and the organic carbon pump in the northern Indian Ocean. *Progress in Oceanography*, *175*, 24–39. https://doi.org/10.1016/j.pocean.2019.03.001

Sirocko, F., Garbe-Schönberg, D., & Devey, C. (2000). Processes controlling trace element geochemistry of Arabian Sea sediments during the last 25,000 years. *Global and Planetary Change*, *26*, 217–303. https://doi.org/10.1016/S0921-8181(00)00046-1

Tripathi, S., Tiwari, M., Lee, J., Khim, B.-K., & IODP. (2017). Expedition 355 ScientistsFirst evidence of denitrification vis-a-vis monsoon in the Arabian Sea since late Miocene. *Scientific Reports*, *7*(1), 1–7. https://doi.org/10.1038/srep43056

Walsh, J. J. (1991). Importance of continental margins in the marine biogeochemical cycling of carbon and nitrogen. *Nature*, *350*(6313), 53–55. https://doi.org/10.1038/350053a0

Wan, S. M., Clift, P. D., Zhao, D. B., Hovius, N., Munhoven, G., France-Lanord, C., et al. (2017). Enhanced silicate weathering of tropical shelf sediments exposed during glacial lowstands: A sink for atmospheric CO_2. *Geochemica et Cosmochimica Acta*, *200*, 123–144. http://dx.doi.org/10.1016/j.gca.2016.12.010

Wan, S. M., Yu, Z. J., Clift, P. D., Sun, H. J., Li, A. C., & Li, T. G. (2012). Tectonic and climatic controls on long-term silicate weathering in Asia since 5 Ma. *Geophysical Research Letters*, *39*, L15611. https://doi.org/10.1029/2012GL052377

Wang, B. S., Zhao, Q. H., & Jian, Z. M. (2005). Changes of organic carbon and paleoproductivity in the southern South China Sea since middle Pliocene. *Marine Geology & Quaternary Geology*, *25*(2), 73–79.(in Chinese with English Abstract).

Weber, M. E., Lantzsch, H., Dekens, P., Das, S. K., Reilly, B. T., Martos, Y. M., et al. (2018). 200,000 years of monsoonal history recorded on the lower Bengal Fan-strong response to insolation forcing. *Global and Planetary Change*, *166*, 107–119. https://doi.org/10.1016/j.gloplacha.2018.04.003

Winckler, G., Anderson, R. F., Jaccard, S. L., & Marcantonio, F. (2016). Ocean dynamics, not dust, have controlled equatorial Pacific productivity over the past 500000 years. *Proceedings of the National Academy of Sciences of the United States of America*, *113*(22), 6119–6124. https://doi.org/10.1073/pnas.1600616113

Xiong, Z. F., Li, T. G., Chang, F. M., Algeo, T. J., Clift, P. D., Bretschneider, L., et al. (2018). Rapid precipitation changes in the tropical West Pacific linked to North Atlantic climate forcing during the last deglaciation. *Quaternary Science Reviews*, *197*, 288–306. https://doi.org/10.1016/j.quascirev.2018.07.040

Xu, Z. K., Li, T. G., Clift, P. D., Wan, S. M., Qiu, X. H., & Lim, D. I. (2018). Bathyal records of enhanced silicate erosion and weathering on the exposed Luzon shelf during glacial lowstands and their significance for atmospheric CO_2 sink. *Chemical Geology*, *476*, 302–315. https://doi.org/10.1016/j.chemgeo.2017.11.027

Xu, Z. K., Wan, S. M., Colin, C., Li, T. G., Clift, P. D., Chang, F. M., et al. (2020). Enhanced terrigenous organic matter input and productivity on the western margin of the Western Pacific Warm Pool during the Quaternary sea-level lowstands: Forcing mechanisms and implications for the global carbon cycle. *Quaternary Science Reviews*, *232*, 106211. https://doi.org/10.1016/j.quascirev.2020.106211

Yu, Z. J., Colin, C., Bassinot, F., Wan, S. M., & Bayon, G. (2020). Climate-driven weathering shifts between highlands and floodplains. *Geochemistry, Geophysics, Geosystems*, *21*, e2020GC008936. https://doi.org/10.1029/2020GC008936

Yu, Z. J., Colin, C., Wan, S. M., Saraswat, R., Song, L. N., Xu, Z. K., et al. (2019). Sea level-controlled sediment transport to the eastern Arabian Sea over the past 600 kyr: Clay minerals and Sr-Nd isotopic evidence from IODP site U1457. *Quaternary Science Reviews*, *205*, 22–34. https://doi.org/10.1016/j.quascirev.2018.12.006

Zhao, G. M., Ye, S. Y., He, L., Yuan, H. M., Ding, X. G., Wang, J., et al. (2020). Historical change of carbon burial in Late Quaternary sediments of the ancient Yellow River delta on the west coast of Bohai Bay, China. *Catena*, *193*, 104619. https://doi.org/10.1016/j.catena.2020.104619

Ziegler, M., Lourens, L. J., Tuenter, E., & Reichart, G.-J. (2010). High Arabian Sea productivity conditions during MIS 13 – odd monsoon event or intensified overturning circulation at the end of the Mid-Pleistocene transition? *Climate of the Past*, *6*, 63–76. https://doi.org/10.5194/cp-6-63-2010